

AGU Advances



RESEARCH ARTICLE

10.1029/2025AV001919

Peer Review The peer review history for this article is available as a PDF in the Supporting Information.

Key Points:

- A robust global separation of anvil and in situ cirrus is achieved using a novel physically constrained computer vision method
- Anvil cirrus extent is tightly coupled to dynamical factors, whereas in situ cirrus is modulated by remote, interhemispheric forcing
- A new interhemispheric teleconnection is revealed, rapidly linking deep convection to opposite-hemisphere in situ cirrus via planetary waves

Supporting Information:

Supporting Information may be found in the online version of this article.

Correspondence to:

J. Ge, gejm@lzu.edu.cn

Citation

Mu, Q., Ge, J., Huang, J., Hu, X., Peng, N., Li, Y., et al. (2025). A new classification of in situ and anvil cirrus clouds uncovers their properties and interhemispheric connections. *AGU Advances*, 6, e2025AV001919. https://doi.org/10.1029/ 2025AV001919

Received 17 JUN 2025 Accepted 16 OCT 2025

Author Contributions:

Conceptualization: Qingyu Mu, Jinming Ge, Jianping Huang Data curation: Qingyu Mu, Jinming Ge, Xiaoyu Hu, Nan Peng, Chi Zhang Formal analysis: Qingyu Mu, Jinming Ge Funding acquisition: Jianping Huang Investigation: Qingyu Mu, Jinming Ge Methodology: Qingyu Mu, Jinming Ge, Jie Zhang

Project administration: Jinming Ge, Jianping Huang

Project Oingun Mu, Jinming Go,

Resources: Qingyu Mu, Jinming Ge, Meihua Wang

© 2025. The Author(s).

This is an open access article under the terms of the Creative Commons

Attribution License, which permits use, distribution and reproduction in any medium, provided the original work is

properly cited.

A New Classification of In Situ and Anvil Cirrus Clouds Uncovers Their Properties and Interhemispheric Connections

Qingyu Mu¹, Jinming Ge¹, Jianping Huang¹, Xiaoyu Hu^{2,3}, Nan Peng¹, Yize Li¹, Meihua Wang⁴, Jie Zhang¹, Ziyang Xu¹, Chi Zhang¹, and Bochun Liu¹

¹Key Laboratory for Semi-Arid Climate Change of the Ministry of Education and College of Atmospheric Sciences, Lanzhou University, Lanzhou, China, ²Chongqing Research Institute of Big Data, Peking University, Chongqing, China, ³School of Mathematical Sciences, Peking University, Beijing, China, ⁴College of Optoelectronic Technology, Chengdu University of Information Technology, Chengdu, China

Abstract The challenge of distinguishing convective anvil cirrus from in situ cirrus has long limited the quantification of their distinct roles in regulating upper-tropospheric moisture and modulating Earth's energy budget. In this study, we address this ambiguity by introducing a physically constrained classification framework that applies advanced computer vision techniques to CloudSat-CALIPSO observations. By tracking the complete physical evolution of cloud systems from their convective origins, this method enables a robust global separation of anvil and in situ cirrus. Our results illuminate stark contrasts in their macro- and microproperties, governed by fundamentally different mechanisms. Anvil cirrus extent is tightly coupled to dynamic factors, whereas in situ cirrus, while linked to local tropopause thermodynamics, exhibits strong modulation by remote atmospheric influences from the opposite hemisphere. This identified linkage shows a previously unrecognized interhemispheric teleconnection: wherein large-scale deep convective systems in one hemisphere rapidly influence in situ cirrus formation in the other. We hypothesize that this coupling is mediated by planetary-scale waves—likely fast-propagating Kelvin waves that transmit energy across the equator, cooling the remote tropical tropopause layer, with subsequent interactions with the subtropical jet fostering mid-latitude in situ development. This newly quantified atmospheric coupling provides a pathway for improving representation of cirrus in climate models and suggests a mechanism by which regional shifts in convection under global warming could reshape global cirrus distributions and their radiative impact.

Plain Language Summary Cirrus clouds—the wispy, high-altitude ice clouds—are critical players in Earth's climate. They form in two main ways: anvil cirrus spread out from large storm systems, while in situ cirrus form on their own, high in the quiet atmosphere. Telling these two types apart on a global scale has been a long-standing challenge. Using an innovative method that applies computer vision to satellite data, we have created the first global maps that cleanly separate these cloud types. Our analysis revealed a surprising connection across the planet: powerful storm systems in one half of the world generate massive atmospheric waves that travel across the equator, significantly influencing the formation of in situ cirrus in the opposite hemisphere. This discovery highlights how interconnected our climate is and confirms that the two cirrus types are governed by different rules. Anvil cloud amount is driven by storm activity in its own hemisphere. In contrast, in situ cloud formation, while dependent on local conditions, is also clearly controlled by major storms thousands of miles away. This newfound coupling is vital for climate models to accurately predict how shifting storm patterns under global warming will reshape our future climate.

1. Introduction

Cirrus clouds, composed of ice crystals in the upper troposphere, fundamentally shape Earth's radiative balance through their unique optical properties. Their thin, filamentous structure allows most solar radiation to pass while efficiently trapping outgoing longwave radiation, producing a net top-of-atmosphere warming that is strongest in the tropics and seasonally variable in midlatitudes (Hong et al., 2016). Multi-sensor flux analyses further confirm that pure ice clouds generally contributing to warming (Matus & L'Ecuyer, 2017). Beyond direct radiative forcing, cirrus clouds regulate upper-tropospheric humidity and mediate stratosphere-troposphere exchange, thereby modulating large-scale atmospheric circulation and precipitation patterns (Corti et al., 2006; Dinh & Fueglistaler, 2014; Jensen et al., 2011).

MU ET AL. 1 of 14

2576604x, 2025, 6, Downloaded from https://agupub

brary.wiley.com/doi/10.1029/2025AV001919 by Lanzhou University, Wiley Online Library on [05/11/2025]. See the

Jinming Ge

Writing - review & editing: Qingyu Mu,

The climate impact of cirrus clouds depends fundamentally on their formation pathway. Following established frameworks (Krämer et al., 2016; Mace et al., 2006), ice clouds in the upper troposphere arise through two distinct mechanisms: (a) liquid-origin cirrus formed through detrainment from deep convective systems—commonly termed anvil cirrus—where ice crystals originate in the moisture-rich lower atmosphere and are lofted upward, and (b) in situ-origin cirrus that nucleate directly in the cold upper troposphere via frontal lifting, orographic forcing, or gravity-wave perturbations. These formation pathways yield systematically different properties and radiative behaviors (Riihimaki & McFarlane, 2010; Zhao et al., 2019). Liquid-origin anvil cirrus, inheriting characteristics from convective processes, tend to be optically thicker and influence both shortwave and longwave radiation, with domain-mean top-of-atmosphere effects often near-neutral due to offsetting warming and cooling (Deutloff et al., 2025; Hartmann & Berry, 2017; McKim et al., 2024). In contrast, in situ-origin cirrus, formed through gradual cooling and vapor deposition, produce thinner, more diffuse layers that regulate uppertropospheric humidity and typically exert net longwave warming (Gasparini et al., 2023; Joos et al., 2008; Luebke et al., 2016). Because these formation controls and radiative responses differ fundamentally, accurately distinguishing anvil from in situ cirrus is essential for attribution, interpreting observed fluxes, and constraining model feedbacks. Yet this distinction presents a fundamental observational challenge: anvil fragments detach from their convective origins during evolution and can exhibit optical properties similar to in situ cirrus, making profile-level separation essential but persistently difficult.

Several classification frameworks have been developed to tackle this challenge, each balancing trade-offs among spatial coverage, temporal evolution, and vertical resolution. Threshold-based methods efficiently classify clouds from satellite retrievals (Mace et al., 2006; McKim et al., 2024), but often misclassify anvil outflow or multilayer in situ clouds due to fixed parameter thresholds. Distance-based approaches enhance spatial context by collocating narrow-swath active sensor with wide-swath geostationary brightness temperatures, yet can conflate optically thick anvils with convective cores and overlook aged anvil remnants (Sokol & Hartmann, 2020). Trajectory-based methods provide a dynamically consistent view by advecting convective air parcels forward using reanalysis winds to trace anvil-to-in situ transition (Horner & Gryspeerdt, 2023), though their accuracy depends on wind fields and threshold choices. While these diverse strategies have advanced cirrus classification, our objective—to quantify the physical contrasts between cirrus types and link them directly to their verticallyresolved meteorological context-requires high-fidelity classification at the profile scale. Without robust observational constraints, models cannot accurately represent distinct microphysics, meteorological responses, or each cirrus type feedback leading to biases that propagate into climate sensitivity estimates (Krämer et al., 2016; Sokol et al., 2024).

Here, we develop a physically-constrained computer vision method that directly addresses this challenge by tracking cloud system evolution from convective origins. Designed for high-fidelity separation on the CloudSat-CALIPSO observation curtain, our approach exploits a fundamental distinction: anvil cirrus maintains a traceable connection to deep convection, while in situ cirrus forms independently in the upper troposphere. By integrating iterative expansion with physical property constraints, this framework captures both attached and detached anvil structures with high confidence. This classification framework provides the vertically-resolved, contour-level foundation necessary to investigate fundamental questions about cirrus-climate interactions: How do macroand microphysical properties differ between anvil and in situ cirrus on a global scale? What specific, co-located meteorological factors control their formation and maintenance? And can atmospheric dynamics forge connections between these distinct cirrus populations across vast spatial scales?

Addressing these questions reveals previously hidden aspects of cirrus behavior that challenge conventional understanding. The two types exhibit fundamentally different properties: anvil cirrus displays large ice crystals with high ice water content concentrated in convective regions, while in situ cirrus shows smaller crystals uniformly distributed globally. These distinct characteristics translate into contrasting meteorological controls anvil cirrus remains tightly coupled to regional convective intensity, whereas in situ cirrus responds to a hierarchy of influences from local upper-tropospheric conditions to remote forcing. Most strikingly, our analysis of large-scale connections uncovers a robust interhemispheric teleconnection: summer-hemisphere deep convection systematically modulates winter-hemisphere in situ cirrus coverage through planetary-scale wave propagation along subtropical jet waveguides. This newly discovered atmospheric bridge reveals cirrus as active participants in a globally interconnected system, transforming our understanding of how regional convective changes under warming will reshape global cirrus distributions and their climate roles. Advancing this understanding is therefore essential for improving the representation of cirrus and their feedbacks in numerical models.

MU ET AL. 2 of 14 AGU Advances 10.1029/2025AV001919

2. Data Set and Method

2.1. Observational and Auxiliary Data Sets

The development of our novel cirrus classification and the ensuing detailed analyses of cloud properties, governing mechanisms, and atmospheric teleconnections are built upon an extensive synthesis of multi-platform satellite observations and auxiliary reanalysis data. Central to this framework is a substantial observational record from the CloudSat-CALIPSO missions, encompassing approximately 21,008 orbital granules over 5-year period from June 2006 to April 2011. Meteorological factors in upper-troposphere from ECMWF Auxiliary Product and aerosol from MERRA-2 are meticulously integrated detailing essential atmospheric state and aerosol influence.

The complementary capabilities of the A-Train's core sensors are essential. CloudSat's 94-GHz Cloud Profiling Radar (CPR) provides sensitive to the larger ice particles, though its signal can be attenuated in optically thick regions or affected by non-Rayleigh scattering from aggregated ice (Heymsfield et al., 2008). Our CPR reflectivity analysis confirms that vast majority of classified cirrus occur well below these high-reflectivity regimes (Text S3.1, Figure S5 in Supporting Information S1). In contrast, CALIPSO's lidar excels at detecting optically thin cirrus and elevated cirrus layers, but becomes fully attenuated at optical depths about three. By combining these complementary sensitivities, our framework captures both anvil and in situ cirrus across a wide range of conditions.

Our analysis integrates synergistic CloudSat-CALIPSO products to progressively refine the cloud information used by the PCIV classifier (Section 2.2). We begin with 2B-CLDCLASS-LIDAR (Sassen et al., 2008) to obtain an initial cloud typing (convective cores and cirrus objects), then sharpen spatial delineation and remove spurious detections with 2B-GEOPROF-LIDAR, which applies a 50% minimum cloud-fraction threshold (Li et al., 2014). With these delineated profiles, 2C-ICE (Deng et al., 2013) provides microphysical fields by combining radar reflectivity and lidar backscatter to estimate ice water content (IWC) and ice-crystal effective radius (γ_e) . To examine meteorological controls, we augment the cloud fields with upper-tropospheric dynamical and thermodynamical variables from ECMWF-AUX (details in Text S1 and Table S1 in Supporting Information S1). To limit aerosol-cloud confounding when analyzing microphysics and meteorological drivers (Sections 3-4), we apply a background-aerosol filter using MERRA-2 total column aerosol optical thickness (TAOT < 0.07; Gelaro et al. (2017); threshold following Chen et al. (2024). Importantly, this aerosol filter is not used by PCIV itself: the classification and all global occurrence statistics are derived from the full, unscreened data set, so the integrity of identified cloud structures and their physical linkages is unaffected by aerosol filtering. Sensitivity tests confirm that our main findings are robust to reasonable choices of the TAOT threshold (Text S5; Figures S11 and S12 in Supporting Information S1). This integrated, yet methodologically segregated, use of cloud, meteorological, and aerosol information underpins our global separation of anvil and in situ cirrus and the subsequent diagnosis of their governing mechanisms.

2.2. Physically Constrained Iterative Vision Method for Cirrus Classification

We proposed a Physically Constrained Iterative Vision (PCIV) method to overcome conventional classification ambiguities and robustly distinguish global in situ and anvil cirrus. The highly fragmented nature of anvil cirrus, which often appear as multiple disconnected segments from their origin convection, poses challenge that conventional methods struggle to establish the linkage between these detached anvil fragments and their origins, leading to systematic misclassification as in situ cirrus. Our method addresses this by leveraging regional connectivity principles from computer vision (Ge et al., 2024; Hu et al., 2021) with synergistic high-resolution CloudSat-CALIPSO observations. The core strategy is tracking the physical evolution of cirrus outflow from identified convective origins while systematically enforcing microphysical and thermodynamic constraints. The PCIV process initiates within each orbital granule by using connected-component labeling to delineate discrete cirrus objects. Concurrently, convective cores, the genesis points for anvil cirrus, are identified from established cloud type information derived from the CloudSat-CALIPSO products.

The full anvil structure is then delineated through an iterative expansion process designed to emulate the physical dispersion of cirrus outflow from these convective sources. A key physical constraint is applied throughout the classification: only cirrus objects with cloud top temperature below -38° C, a threshold for homogeneous ice nucleation (Krämer et al., 2016), are considered. Initially, potential anvil segments are identified as cirrus objects

MU ET AL. 3 of 14

2576604x, 2025, 6, Downloaded from https://agupubs.onlinelibrary.wiley.com/doi/10.1029/2025AV001919 by Lanzhou University, Wiley Online Library on [05/11/2025]. See the Terms and Conditions (https://online

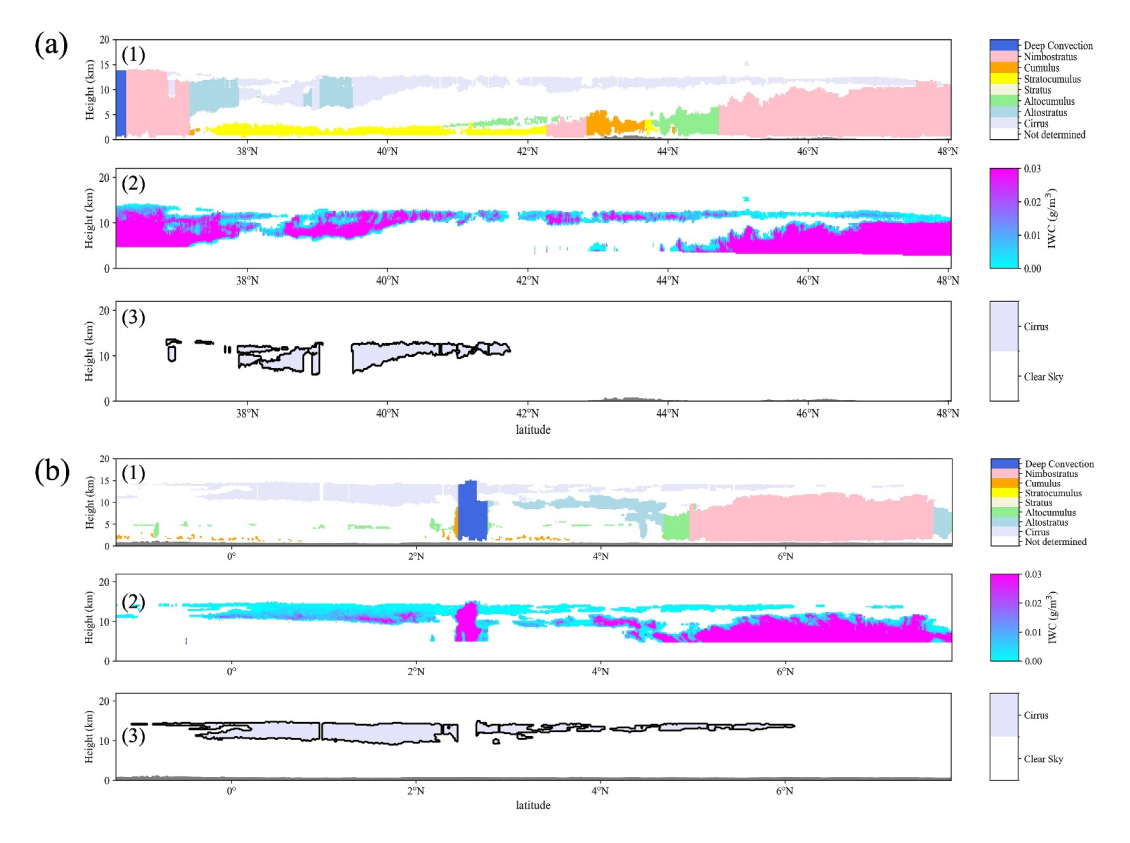


Figure 1. Case studies demonstrating the PCIV methodology for cirrus classification. Two orbital granules are presented: (a) 15 June 2006 at 03:18 UTC and (b) 28 June 2006 at 11:02 UTC. For each case, three subpanels display: (1) the initial cloud type classification from 2B-CLDCLASS-LIDAR, (2) IWC distribution for detected clouds, and (3) the final anvil structures identified by the PCIV algorithm. The methodology tracks anvil outflow from convective cores while distinguishing detached segments.

located within 5 km horizontally (approximately triple the CloudSat along-track resolution) and 240 m vertically of a detected convective core. Starting from these segments, an iterative cycle of morphological dilation and rigorous physical validation is applied. In each iteration, the spatial domain surrounding the existing anvils is expanded by 5 km horizontally and 240 m vertically to search for neighboring cirrus objects. These candidates are incorporated into the growing anvil structure only if they meet an additional physically motivated criterion: a mean IWC not exceeding 1.2 times that of the parent anvil segment from which it is expanding. This IWC constraint preserves consistency with observed anvil dispersion and microphysical evolution (Sokol et al., 2024). The expand–validate–merge cycle proceeds until no additional qualifying cirrus are found, yielding physically coherent anvil structures (Figure S1 in Supporting Information S1).

After anvil delineation converges, remaining cirrus objects satisfying the -38°C criterion and vertically separated from underlying cloud by ≥ 5 km (Text S3.3; Figure S7 in Supporting Information S1) are classified as in situ. Sensitivity tests around this threshold (2, 3, 5 km) showed negligible classification impact; we retain 5 km to limit contamination from overlapping systems. This operational framework thus partitions upper-tropospheric ice based on observable convective linkage: anvil cirrus captures the liquid-origin pathway via deep convection, while in situ cirrus represents all other formation mechanisms. Although the in situ category is composite—including true in situ nucleation, weaker liquid-origin cirrus from non-DCS sources (e.g., extratropical cyclones), and occasional contrails—these diverse pathways share a common defining characteristic: absence of connection to organized deep convection. This shared attribute produces coherent meteorological signatures distinct from anvil cirrus (Text S3.4; Figures S8 and S9 in Supporting Information S1), validating the classification's utility for diagnosing formation controls despite the in situ category's internal diversity.

Applied to the 5-year CloudSat-CALIPSO record, the PCIV algorithms yields a globally consistent separation of anvil and in situ cirrus. Figure 1 illustrates advantages over threshold- or proximity-only schemes. In the first orbit

MU ET AL. 4 of 14



(Figure 1a), panel (1) shows the baseline cloud types, panel (2) the IWC field, and panel (3) the PCIV anvil mask. A threshold-only optical-depth approach would merge the anvil with a nearby in situ layer near ~46°N because the two exhibit similar IWC and optical properties; PCIV keeps them distinct by requiring dynamical connectivity to a convective core and consistent temperature/IWC evolution. In another case (Figure 1b), the algorithm recovers detached anvil clusters that proximity-only methods miss, because the segments continue to satisfy the outflow-based physical constraint.

While these examples highlight the method's strengths in resolving ambiguities, we also systematically assessed its potential limitations, including CALIOP attenuation at $\tau \approx 3$, the CloudSat 94-GHz "dim band" near outflow (Heymsfield et al., 2008), and IWC continuity that may exclude portions of anvils under variable moisture. Because PCIV excludes precipitating cores and enforces smooth T–IWC continuity, any resulting bias primarily shortens core-adjacent anvil segments rather than misclassifying them as in situ. Furthermore, aviation-induced thin cirrus may appear within the in situ category, reflecting our operational design based on the physical distinction between "in situ origin" and "liquid origin" cirrus (Krämer et al., 2016). Only liquid-origin cirrus with traceable convective link are classified as anvil, while other ice clouds including contrails or synoptic cirrus fall into the broader "in situ" category. Crucially, excluding the typical NH contrail cruise layer (\approx 250–180 hPa, Gryspeerdt et al., 2024; Teoh et al., 2024) does not alter key in situ statistics or the central teleconnection result (Text S4, Figure S10 in Supporting Information S1). Although our curtain-based approach also faces potential influence from off-swath convective sources, supplementary analyses confirm overall robustness (Text S3.2, Figure S6 in Supporting Information S1). Therefore, the combination of convective-core tracking, iterative expansion, and physically grounded constraints yield a dynamically self-consistent classification that reliably supports analyses of cirrus meteorological controls and atmospheric interactions.

2.3. Meteorological Drivers Framework for Different Cirrus

The globally consistent distribution of in situ and anvil cirrus enabled by our method provides a robust foundation for investigating the distinct meteorological drivers of each cirrus type. We employed ridge regression to address multi-collinearity inherent in chosen meteorological variables (Figure S2 in Supporting Information S1). These variables exhibited substantial inter-correlation (often >0.5), rendering ordinary regression methods unreliable. Ridge regression mitigates this issue through L2 regularization, which penalizes large coefficient magnitudes by adding a term proportional to the sum of squared coefficients. This approach preventing overfitting to correlated variables, while retaining all predictors in the model, enabling a more stable and interpretable estimation of each variable's relative influence.

Cirrus occurrence frequency was calculated on a $3^{\circ} \times 3^{\circ}$ grid at 16-day intervals, aligning with the CloudSat-CALIPSO repeat cycle. Following the 3S-GEOPROF-COMB methodology (Bertrand et al., 2024), this frequency was defined as the ratio of satellite profiles containing a specific cirrus type to the total number of valid profiles within each grid cell. We then used ridge regression model to reconstruct cirrus frequencies as a function of standardized meteorological predictors. The optimal penalty strength ($\lambda = 12$) was selected via cross-validation across a range from logarithmic range from 10^{-3} to 10^{3} and applied uniformly. Regressions were conducted independently for each grid cell, and only those with positive coefficients of determination ($R^{2} > 0$) and correlation coefficients exceeding 0.4 were retained for further analysis (Andersen et al., 2023). This procedure yields a stable, statistically robust characterization of the contrasting meteorological sensitivities of in situ and anvil cirrus, with skill metrics and coefficient patterns effectively unchanged between daytime and nighttime overpasses (Text S6; Figures S13 and S14 in Supporting Information S1).

3. Macro- and Microphysics of In Situ and Anvil Cirrus

Applying our classification to 5 years of CloudSat–CALIPSO observations, Figure 2 presents the global distributions of anvil and in situ cirrus and their distinct morphological and microphysical characteristics. In situ cirrus exhibits a broadly continuous spatial pattern from the tropics to high latitudes, with a modest enhancement near the equator (10°S–10°N). This homogeneity is consistent with the wide availability of upper-tropospheric formation pathways (e.g., synoptic-scale ascent and gravity-wave cooling). Vertically, their occurrence maximizes a few kilometers below the local tropopause and shifts with latitude (Figure 2a, left panel, red line), consistent with enhanced cirrus formation linked to the tropical tropopause layer (TTL) (Lamraoui et al., 2023; Lesigne et al., 2024). Importantly, our classification also detects ultra-thin layers that hug the tropopause, with rare,

MU ET AL. 5 of 14

2576643x, 2025, 6, Downloaded from http://agupubs.onlielibrary.wiley.com/doi/10.1029/2025AV0001919 by Lazabou University, Wiley Online Library on [05/11/2025]. See the Terms and Conditions (https://onlinelibrary.wiley.com/terms-and-conditions) on Wiley Online Library from less of use; OA articles are governed by the applicable Creative Commons Licensware.

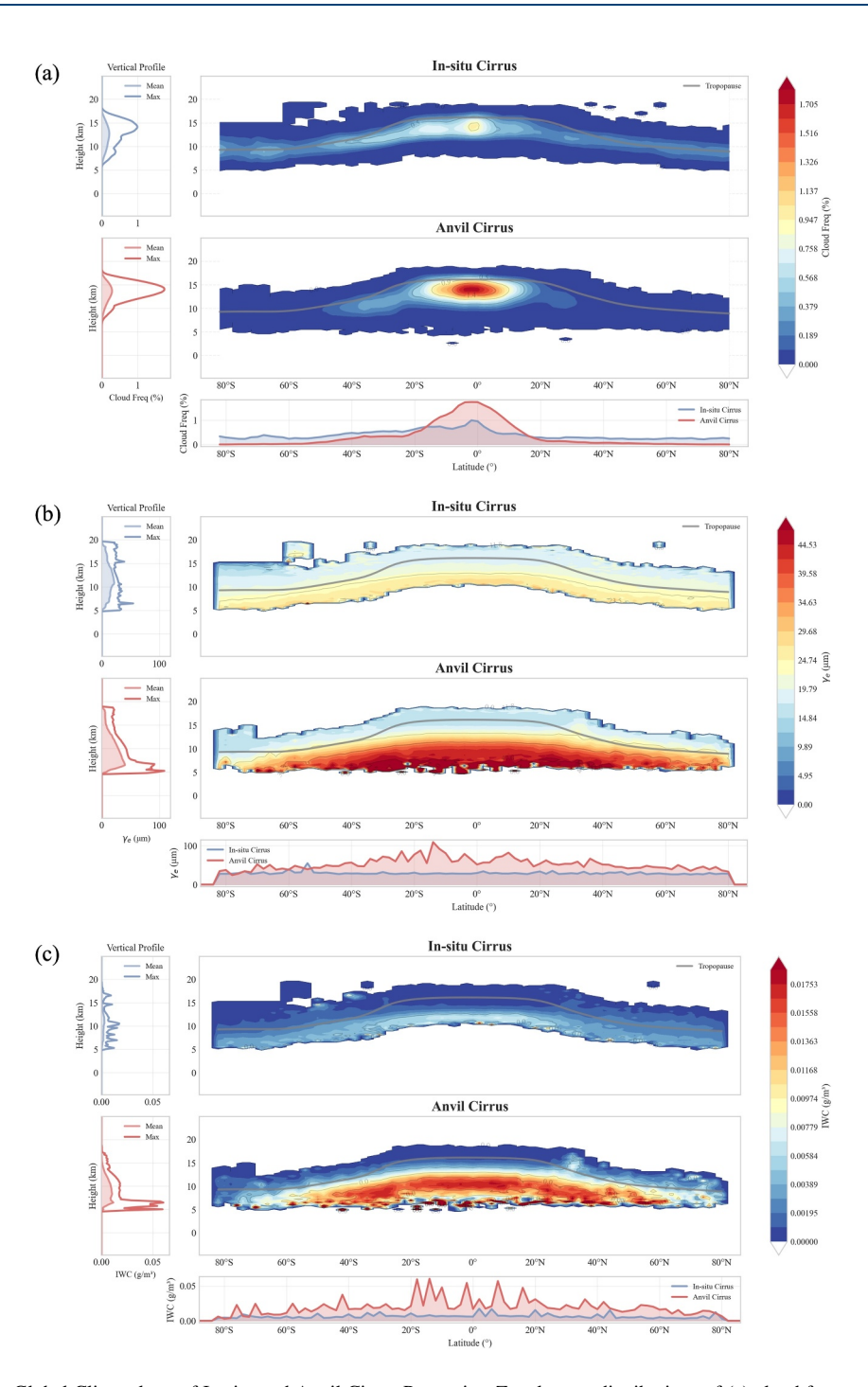


Figure 2. Global Climatology of In situ and Anvil Cirrus Properties. Zonal mean distributions of (a) cloud frequency (%), (b) ice crystal effective radius (γ_e , μ m), and (c) ice water content (IWC, g/m³) for in situ cirrus (top row) and anvil cirrus (middle row), derived from 5 years (2006–2011) of CloudSat-CALIPSO observations. Cloud occurrence frequency is calculated as the ratio of profiles containing the specified cirrus type to the total number of valid atmospheric profiles. In each panel, the left-side inset displays the mean vertical profile, while the bottom-plot shows the vertically integrated latitudinal distribution. The contrasting distributions of frequency, particle size, and ice content highlight the fundamentally different formation pathways and characteristics of the two cirrus types with the tropopause height indicated by a solid gray line.

episodic excursions into the lowermost stratosphere during strong gravity-wave activity. These features are consistent with the subvisual cirrus documented by OSIRIS/Odin (Bourassa et al., 2005). They should not be interpreted as a persistent mid-latitude 17–18 km "mode"; when mapped in tropopause-relative coordinates they

MU ET AL. 6 of 14

2576604x, 2025, 6, Downloaded from https://agupubs.onlinelibrary.wiley.com/doi/10.1029/2025AV001919 by Lanzhou University, Wiley Online Library on [05/11/2025]. See the Term

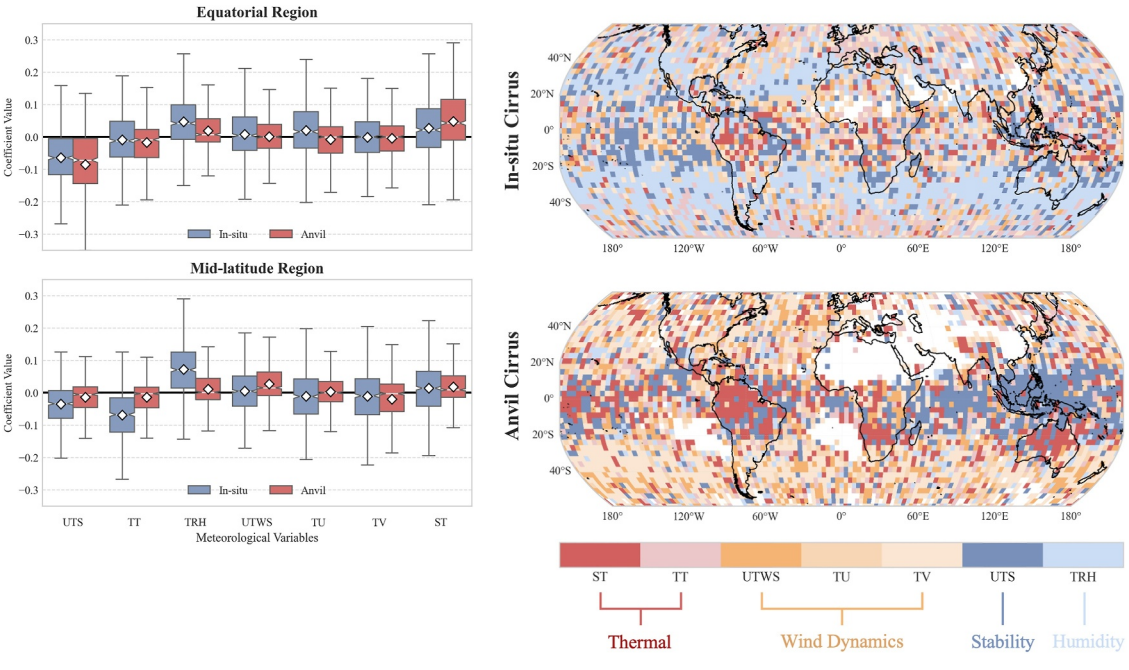


Figure 3. Meteorological controls on cirrus occurrence from ridge regression using curtain-collocated ECMWF-AUX fields. (a) Equatorial (20°S–20°N, top) and midlatitude (20°–60°, bottom) bands: box-and-whisker plots of standardized coefficients for in situ (blue) and anvil (red) cirrus; boxes span the interquartile range across retained grid cells, diamonds mark medians, and whiskers show the 10–90th percentiles; (b) Global maps of the locally dominant factor for in situ (top) and anvil (bottom) cirrus, defined as the predictor with the largest absolute standardized coefficient at each grid cell; colors group variables into Thermal (ST, TT), Wind dynamics (UTWS, TU, TV), and Stability/Humidity (UTS, TRH).

sit within \sim 1 km of the local dynamical/thermal tropopause and comprise only a very small fraction of detections. While aviation-induced cirrus can contribute thin layers, typical cruise levels (\sim 250–180 hPa; Singh et al., 2024) lie well below these UTLS heights, making contrails an unlikely explanation for this feature. In contrast, anvil cirrus is concentrated in the deep-convection belt (\approx 30°S–30°N), with maxima over Southeast Asia, the Western Pacific warm pool, and the Indian Ocean (Figures 2a and 4a, right panels), where warm SSTs and abundant moisture sustain persistent convection. The vertical extent of anvils captured by our methodology exceeds prior estimates (e.g., Riihimaki & McFarlane's, 2010) because our object-centered approach preserves both overshooting tops and detached lower segments. This provides a more complete view of anvil lifecycle and microphysical evolution, linking observed macrostructure with co-retrieved IWC and effective radius.

These morphological distinctions are enhanced by contrasting microphysical properties that further differentiate anvil and in situ cirrus categories (Figure 2b). In situ cirrus is featured by relatively small ice crystals near the tropopause, with particle size increasing toward the cloud base (Figure 2b, left panel). Although their vertical extent broadly overlaps with that of anvil cirrus, in situ cirrus does extend to slightly higher altitudes (Figure 2b, left panel, red line). The uniform latitudinal distribution in both γ_e and IWC suggests that in situ cirrus formation depends on supersaturation conditions, which are commonly met in the upper troposphere globally. In contrast, anvil cirrus display more pronounced latitudinal and vertical microphysical variability. Anvil cirrus γ_e is larger at lower altitudes, decreasing with height similar to in situ cirrus. However, anvil cirrus exhibits a distinct equatorial γ_e maximum, with sizes notably larger than in situ cirrus at similar altitudes (Figure 2b, right panel). This equatorial γ_e enhancement diminishes rapidly with altitude; above 15 km equatorially, anvil γ_e can be smaller than that of co-located in situ cirrus, a size difference reflecting their distinct origins: in situ growth via tropopause supersaturation versus anvil development from convective outflow. Furthermore, at mid-latitudes, convective outflow dynamics can lead to anvil cirrus having larger γ_e than in situ cirrus, even at higher altitudes.

Similarly, anvil cirrus IWC is substantially larger than that of in situ cirrus, with pronounced maxima near the equator and evident in some mid-latitude regions (Figure 2c, right panel). This elevated anvil IWC stems from a fundamentally different formation pathway: anvil ice crystals predominantly form and grow in the moisture-rich lower and middle sections of convective updrafts where temperatures are warmer. They are then transported

MU ET AL. 7 of 14

2576604x, 2025. 6, Downloaded from https://agupubs.onlinelibrary.wiley.com/doi/10.1029/2025AV001919 by Lanzhou University, Wiley Online Library on [05/11/2025]. See the Terms

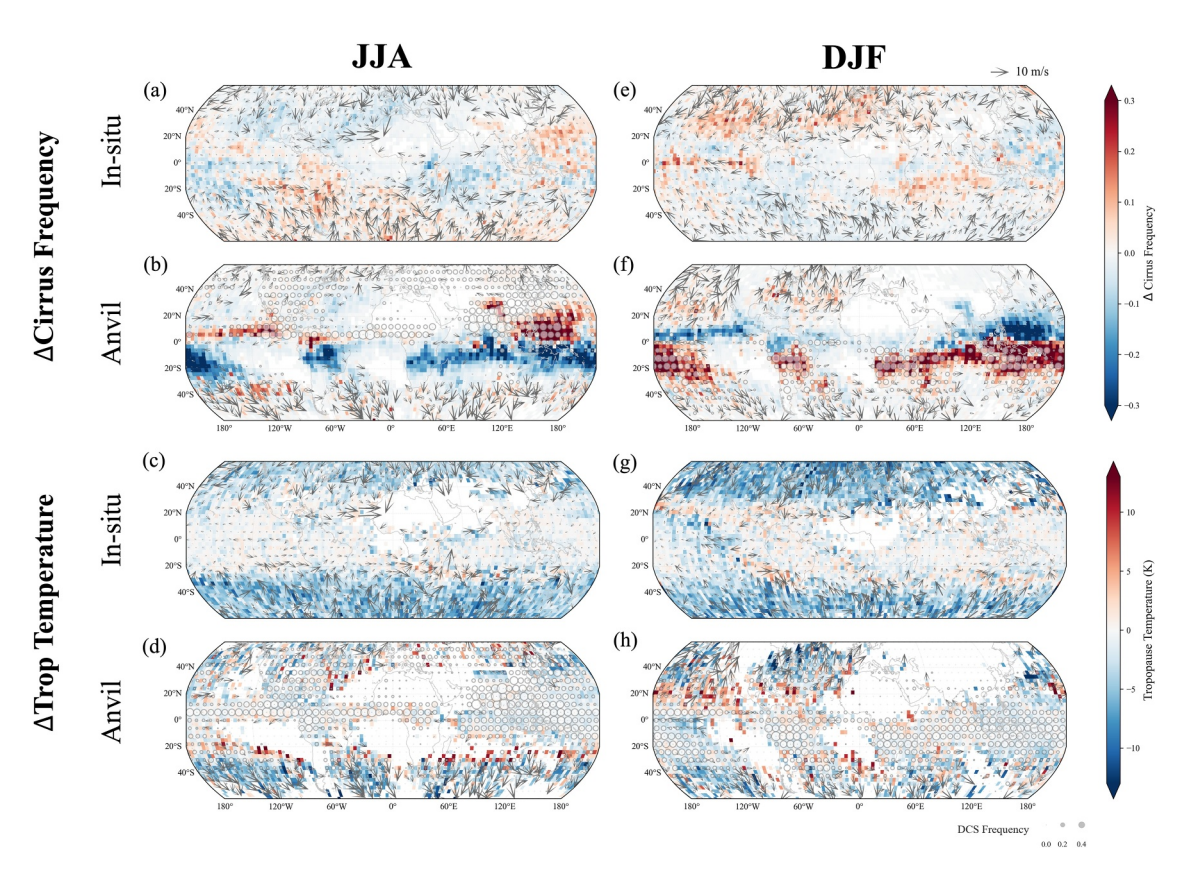


Figure 4. Seasonal anomaly patterns of cirrus frequency and associated tropopause conditions for boreal summer (JJA, left column) and boreal winter (DJF, right column). Panels show frequency anomalies for in situ cirrus in JJA (a) and DJF (e), and anvil cirrus in JJA (b) and DJF (f). Corresponding tropopause temperature anomalies are displayed for in situ cirrus in JJA (c) and DJF (g), and anvil cirrus in JJA (d) and DJF (h). Arrows in all panels indicate concurrent tropopause wind anomalies (scale in upper right corner of each subplot); circles in anvil cirrus panels (b, d, f, h) mark DCS frequency (scale in lower right corner of each subplot).

vertically to the cold upper troposphere and detrained. In contrast, in situ crystals nucleate directly at very cold temperatures and high supersaturations, where significantly less water vapor is available to support substantial growth. Consistent with their γ_e patterns, mid-latitude anvil cirrus can also show higher IWC at greater altitudes compared to typical in situ values, reinforcing the role of strong vertical transport from these distinct, lower-altitude origins. These pronounced morphological and microphysical differences—particularly the larger, more variable particle sizes and significantly higher IWC in anvil cirrus—strongly indicate that anvil and in situ cirrus are governed by distinct meteorological conditions, thereby justifying the quantitative investigation of these mechanisms in subsequent sections.

4. Distinct Meteorological Controls and Hemispheric Teleconnections

4.1. Contrasting Meteorological Controls on In Situ Versus Anvil Cirrus

Building on the distinct properties identified for in situ and anvil cirrus, we applied the ridge regression framework to quantify the meteorological controls on their respective frequencies. Model performance was evaluated by comparing predicted cirrus frequencies against observations (see Supplementary Material Figure S3 and Table S2 in Supporting Information S1). The results demonstrate strong and statistically significant correlations (typically > 0.4) and substantial coefficients of determination (R^2 generally > 0.3) across most regions. Furthermore, global performance metrics—including mean squared error (MSE), mean absolute error (MAE), and average R^2 —consistently support the reliability of the regression framework, confirming its suitability for identifying key meteorological drivers of cirrus occurrence.

Figure 3 presents these controls comprehensively, with the left panels showing regionally averaged coefficients as box plots and the right panels displaying spatial distributions of dominant factors. In equatorial regions (20°S–20°N), upper-tropospheric stability (UTS) emerges as a primary control for both cirrus types as depicted in the

MU ET AL. 8 of 14

upper right panel. This underscores the tropical thermal structure's fundamental role in regulating atmospheric vertical motion, impacting both anvil cirrus and in situ cirrus. However, secondary controls diverge significantly. In situ cirrus exhibits strong dependence on tropopause relative humidity (TRH), then tropopause zonal wind (TU) and surface temperature (ST), suggesting formation linked to upper-level moisture modulated by winds (Li et al., 2018). Conversely, the next most influential factor for equatorial anvil cirrus is ST. Its strong positive coefficient highlights their direct connection to the surface-based thermodynamic engine—warmer ocean surface—that fuels the deep convection from which they originate. These evidence indicate that both types respond to tropical tropospheric stability, while anvil cirrus connect directly to convection's energy source, in situ cirrus primarily respond to upper-tropospheric temperature and moisture conditions.

Right panels in Figure 3 present the spatial distribution of the dominant controlling factors for each cirrus type, highlighting regional variations in their relative influence. For in situ cirrus (top right panel), the maps reveal a clear hemispheric asymmetry in their secondary meteorological drivers: humidity-related factors tend to dominate in the Southern Hemisphere, whereas dynamic and thermodynamic factors appear more influential in the Northern Hemisphere. In the case of mid-latitude anvil cirrus, it shows strong influences from wind dynamic factors, notably meridional wind and wind shear. This points to a transport-dominated formation mechanism, linking cirrus to tropical or subtropical convective outflow. These observed systematic differences in the primary meteorological controls for in situ versus anvil cirrus, and the variations in these controls with latitude, underscore their fundamentally distinct formation pathways. The observed diversity in regional meteorological drivers necessitates a deeper examination of large-scale atmospheric processes to elucidate the underlying causes of these varied controlling pathways.

4.2. Contrasting Hemispheric Controls on Different Cirrus

To better examine the relationship between cirrus and their meteorological environment across spatial and temporal scales, we convert all variables into anomalies, thereby removing their inherent seasonal cycles and spatial gradients. This analysis reveals distinct seasonal structures and highlights the influence of controlling factors over large-scale regions. While cirrus frequency provides a general view of cloud distribution, it does not fully capture the physical scale of cirrus development, which can obscure connections to underlying meteorological drivers. The seasonal anomaly patterns illuminate fundamental differences in how each cirrus type responds to its environment, which are not fully resolved by frequency data alone. In situ cirrus frequency anomalies peak in their respective winter hemisphere (Figures 4a and 4e) under anomalously cold tropopause conditions (Figures 4c and 4g), consistent with primary formation driven by local thermodynamics. This winterhemisphere enhancement reflects the favorable conditions created by enhanced tropopause cooling and increased supersaturation. Anvil cirrus frequency anomalies, though dominated by summer hemisphere convective outflow (Figures 4b and 4f), also show weak positive anomalies in the winter mid-latitudes. These winter anomalies are associated with poleward wind anomalies and suggestive wave-like tropopause temperature patterns (Figures 4d and 4h), hinting at dynamical transport processes extending beyond local convection.

To address the limitations of frequency metrics, we leverage the along-track length of cirrus systems, a metric for which our classification method is particularly well-suited due to its ability to capture the complete spatial structure of each cloud type. We define two key length metrics (visualized in Figure 5): the length of in situ cirrus systems and the length of Deep Convective Systems (DCS)—the organized convective cores that generate anvil cirrus. In this framework, longer in situ cirrus length indicates broader regions influenced by favorable uppertropospheric processes, while longer DCS length serves as a robust proxy for more intense and organized convective activity and its associated latent heat release.

Deseasonalized cirrus length time series reveal markedly different relationships between cirrus horizontal extent and DCS length across hemispheres for the two cirrus types. For anvil cirrus, the analysis demonstrates strong within-hemisphere coupling: correlations between DCS lengths and anvil cirrus lengths are robust when both occur in the same hemisphere (r=0.85 SH, r=0.67 NH, p<0.05 for both), while opposite-hemisphere correlations remain negligible ($r\approx0.1$ –0.2). This pattern confirms that anvil cirrus horizontal extent is tightly governed by the intensity and organization of same-hemisphere deep convection. The analysis of preferred meteorological states (Figures 4d and 4h) further suggests that while local convection dominates, transport along organized flow patterns may modulate their spatial distribution. In contrast, the length-based analysis for in situ cirrus reveals an unexpected pattern: NH in situ cirrus lengths correlate strongly with SH DCS lengths (Figure 5a,

MU ET AL. 9 of 14

10.1029/2025AV001919

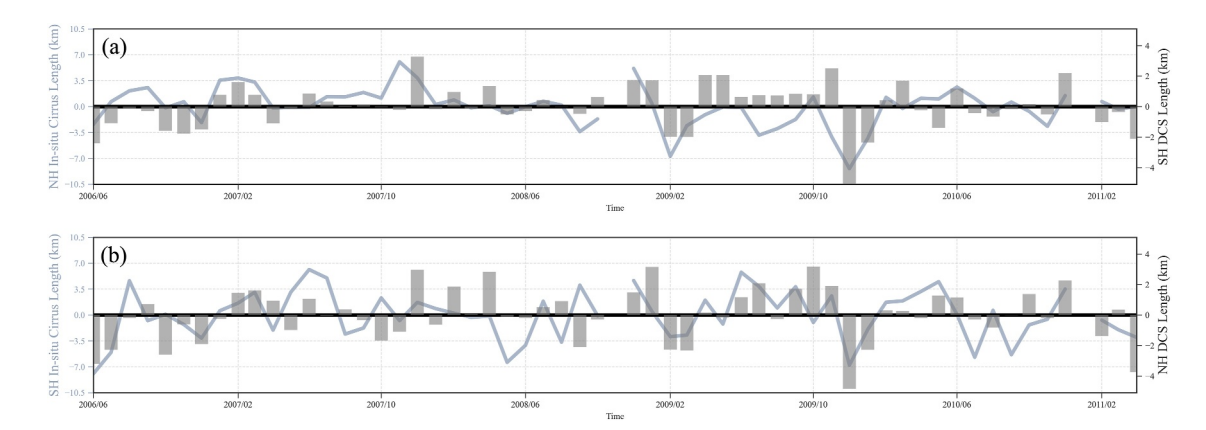


Figure 5. Deseasonalized time series of in situ cirrus and DCS lengths from June 2006 to February 2011. In each panel, the blue line represents the length of in situ cirrus in one hemisphere, and the gray bars indicate DCS lengths in the opposite hemisphere. (a) Northern Hemisphere (NH) in situ cirrus length with Southern Hemisphere (SH) DCS length. (b) SH in situ cirrus length with NH DCS length. This configuration highlights potential cross-hemispheric relationships between in situ cirrus and deep convection.

r = 0.65, p < 0.05), and SH in situ cirrus lengths similarly correlate with NH DCS lengths (Figure 5b, r = 0.46, p < 0.05). Notably, within-hemisphere correlations between DCS and in situ cirrus lengths are much weaker ($r \approx 0.2$, not significant). These strong same-hemisphere coupling of anvil versus opposite-hemisphere coupling of in situ with DCS lengths suggest strikingly different mechanisms and point toward the existence of large-scale dynamical processes.

5. Discussion: Interhemispheric Coupling via Planetary Wave Dynamics

To spatially quantify the teleconnection identified in Section 4.2, we correlate summer-hemisphere convective activity with winter-hemisphere in situ cirrus development. We first construct a summer hemispheric-mean DCS index to represent aggregate convective intensity. This index is calculated by averaging the total along-track length of all DCS within the hemisphere, weighted by the cosine of latitude to account for meridional convergence (see Text S2 in Supporting Information S1 for details). Correlating this deseasonalized DCS index with local, grid-point in situ cirrus length anomalies in the opposite winter hemisphere reveals a statistically significant pattern (Figure 6): a zonally elongated band of positive correlation along the mid-latitude "waveguide" region (20°–40°), a signature consistent with planetary-scale wave activity. This pattern is not an artifact of aviation, as it remains unchanged when potential contrail layers are removed from the analysis (Text S4, Figure S10 in Supporting Information S1). The near-simultaneous nature of this correlation at monthly resolution, showing no substantial lead or lag, provides compelling evidence for rapid cross-equatorial influence occurring on timescales of days to weeks, strongly implicating atmospheric wave dynamics as the primary mediating mechanism. To assess potential interference from contrails, which cluster along aviation routes in mid-latitudes, we recomputed the correlations with cruise layers masked (see Text S3). The pattern shows no observable change, indicating negligible impact from contrails on the teleconnection.

Based on the observed correlation patterns and established atmospheric-dynamics theory, we posit an interhemispheric pathway initiated by summer-hemisphere DCS. Organized convection acts as a sustained elevated heat source, producing upper-tropospheric divergence that excites planetary-scale equatorial wave responses (Gill, 1980; Matsuno, 1966). Among these, equatorially trapped, eastward-propagating Kelvin waves offer a dynamically direct conduit: their gentle, large-scale ascent cools the TTL adiabatically (Wheeler & Kiladis, 1999), lowering temperatures and preconditioning broad regions for ice supersaturation. This sequence aligns with the persistent, hemispheric-scale coupling between convection and in situ cirrus in our multi-year anomalies (Figures 4 and 5) and with prior evidence that Kelvin waves modulate TTL thermal structure on synoptic–intraseasonal timescales (Boehm & Verlinde, 2000; Virts & Wallace, 2014).

The spatial selectivity of the response—an enhancement of in situ cirrus largely confined to the winter-hemisphere 20°–40° band (Figure 6)—implies an additional stage in which equatorial wave energy projects poleward onto the subtropical jet. In this view, the jet acts as a meridional waveguide that can amplify incident disturbances into quasi-stationary trough–ridge trains. The ascent branches of these wave trains preferentially

MU ET AL. 10 of 14



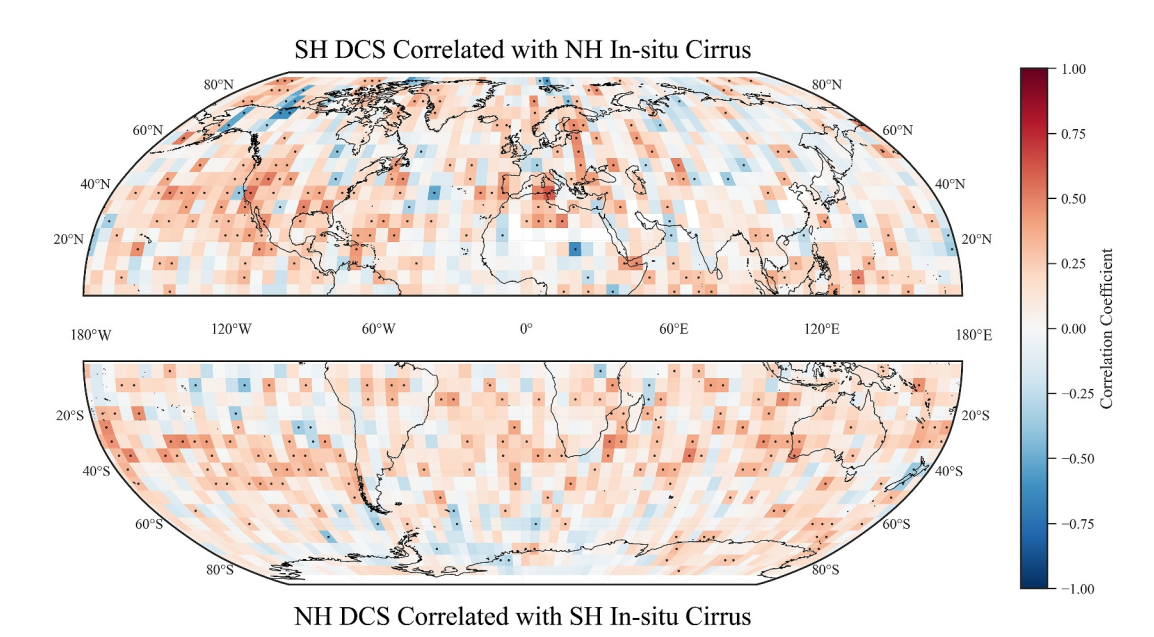


Figure 6. Cross-hemispheric teleconnection between DCS and in situ cirrus revealed through correlation analysis. Grid-point correlation coefficients are shown between deseasonalized in situ cirrus length anomalies and the opposite-hemisphere DCS length index (cosine-weighted hemispheric mean). The upper panel displays correlations between Southern Hemisphere DCS activity and Northern Hemisphere in situ cirrus, while the lower panel shows the reverse relationship. Black dots indicate statistical significance at p < 0.05.

raise upper-tropospheric relative humidity on the jet's equatorward flank, imprinting a midlatitude teleconnection pattern that matches the zonal, band-limited structure in Figure 6. The multi-week propagation and adjustment times intrinsic to this Kelvin-to-jet pathway are consistent with the near-zero-lag relationships resolved at monthly cadence, while the hemispheric scale of both the convective forcing and the jet response explains why an aggregate convection metric projects onto large-scale in situ cirrus development across the opposite hemisphere. This mechanism also clarifies the contrasting behaviors of the two cirrus types diagnosed here. Anvil cirrus remains tightly coupled to local DCS because its microphysics and geometry are governed by detrainment in the same hemisphere, whereas in situ cirrus responds to remotely driven TTL thermodynamics set by the wave field. In other words, the same convective forcing that sets local anvil extent can, via the equatorial-wave/jet sequence, modulate far-field supersaturation and ice initiation conditions in the opposite hemisphere. Although our observational analysis cannot isolate each dynamical component on its own, the combined evidence—hemispheric reach, band-limited midlatitude focus, monthly-scale coherence, and the distinct anvil versus in situ sensitivities—most parsimoniously supports the Kelvin-wave—to-subtropical-jet pathway described above.

6. Conclusions and Implications

This study introduces a novel classification framework, leveraging physically-constrained computer vision on CloudSat-CALIPSO observations, to achieve a robust, global-scale separation of anvil and in situ cirrus. This approach, which tracks the physical evolution of cloud systems from convective sources, overcomes key ambiguities inherent in traditional classification techniques. The resulting classification reveals fundamentally distinct macro- and microphysical characteristics: anvil cirrus displays high ice water content concentrated in deep convective regions, while in situ cirrus exhibits a broader distribution with properties tightly linked to tropopause-level thermodynamics. Further analysis quantifies their contrasting meteorological controls, showing that anvil cirrus extent is tightly coupled to and scales directly with the intensity of same-hemisphere deep convection. In stark contrast, in situ cirrus is significantly influenced by remote atmospheric processes. This key distinction enabled the subsequent identification of a previously unquantified interhemispheric teleconnection: the extent of in situ cirrus in the winter hemisphere is rapidly modulated by the aggregate intensity of DCS in the opposite summer hemisphere, a linkage we hypothesize is mediated by fast-propagating planetary-scale waves.

MU ET AL. 11 of 14

2576604x, 2025, 6, Downloaded from https://agupub

brary.wiley.com/doi/10.1029/2025AV001919 by Lanzhou University, Wiley Online Library on [05/11/2025]. See the Terms

These findings offer a clear path forward for resolving persistent uncertainties in high-cloud representation, from fundamental parameterizations to large-scale feedback assessments. Our work provides the crucial observational constraints needed for GCMs to advance beyond simplified schemes that do not distinguish between these physically distinct cirrus types. By providing a quantitative blueprint of their distinct governing mechanisms—local versus remote—we establish a basis for more physically realistic cloud simulations. This refined separation is critical for accurately assessing high cloud feedbacks in models. While a powerful framework like the Fixed Anvil Temperature (FAT) hypothesis (Hartmann & Larson, 2002) is well-suited for anvil cirrus, our analysis demonstrates it is fundamentally ill-suited for in situ cirrus, whose behavior is tied to remote dynamical modulation. The critical issue arises in models that lack the process-level physics to separate these pathways: they inevitably conflate the two cirrus types, producing a single, blended high-cloud response. Such composite feedback, which artificially averages distinct physical behaviors, will invariably be biased and misrepresent the true climate sensitivity, highlighting the need for the process-level disentanglement our study enables.

Perhaps most critically, the discovery of the interhemispheric teleconnection reveals a planetary-scale pathway of climate influence that is especially important in the context of global warming. Climate projections consistently indicate that deep convection will intensify and shift geographically (Diffenbaugh et al., 2013; Zhang, 2023). Our findings demonstrate that such regional changes can rapidly trigger global consequences through this wave-mediated coupling—a process often underrepresented in models. As summer-hemisphere convection patterns evolve, they will reshape in situ cirrus distributions in the opposite hemisphere, altering global cloud radiative forcing in ways that purely local feedback analyses cannot predict. Incorporating this dynamic linkage into next-generation models is therefore essential for reducing a key uncertainty in climate projections and for anticipating how the globally interconnected climate system will respond to ongoing warming.

Conflict of Interest

The authors declare no conflicts of interest relevant to this study.

Data Availability Statement

Code implementing the PCIV classification and the exact scripts used to generate the figures, together with the processed plotting data supporting the main results, are archived on Zenodo (Mu, 2025, DOI: https://doi.org/10.5281/zenodo.17268605). The CloudSat-CALIPSO observations and auxiliary meteorological data were obtained from the CloudSat Data Processing Center, including 2B-CLDCLASS-LIDAR (https://www.cloudsat.cira.colostate.edu/data-products/2b-cldclass-lidar) for initial cloud-type classification, 2B-GEOPROF-LIDAR (https://www.cloudsat.cira.colostate.edu/data-products/2b-geoprof-lidar) for refined cloud structures, 2C-ICE (https://www.cloudsat.cira.colostate.edu/data-products/2c-ice) for ice water content and effective radius, and ECMWF-AUX (https://www.cloudsat.cira.colostate.edu/data-products/ecmwf-aux) for temperature, humidity, wind, stability, and tropopause height. The MERRA-2 tavg1_2d_aer_Nx aerosol data set (https://data.nasa.gov/dataset/merra-2-tavg1-2d-aer-nx-2d1-hourlytime-averagedsingle-levelassimilationaerosol-diagnostics-b1b07) from NASA's Goddard Earth Sciences Data and Information Services Center (GES DISC) (Global Modeling And Assimilation Office & Pawson, 2015) was used to exclude cases with total aerosol optical thickness above 0.07. All data sets and code are publicly available and fully comply with AGU's open research and data sharing policy.

This research is supported by the National Natural Science Foundation of China (Grant 42427804), the Fundamental and Interdisciplinary Disciplines Breakthrough Plan of the Ministry of Education of China, and the Science and Technology Program of Gansu Province (Grant 24JRRA490). The author thanks Prof. Kazuaki Kawamoto (Nagasaki University) for his insights during the formative stages of this research. The author is also grateful to Dr. Lucia Deaconu (Babes-Bolyai University) and Dr. Zeen Zhu (Brookhaven National Laboratory) for their suggestions during the manuscript's refinement phase. All data supporting this study are openly available in the Open Research section

Acknowledgments

References

Andersen, H., Cermak, J., Douglas, A., Myers, T. A., Nowack, P., Stier, P., et al. (2023). Sensitivities of cloud radiative effects to large-scale meteorology and aerosols from global observations. *Atmospheric Chemistry and Physics*, 23(18), 10775–10794. https://doi.org/10.5194/acp-23-10775-2023

Bertrand, L., Kay, J. E., Haynes, J., & de Boer, G. (2024). A global gridded dataset for cloud vertical structure from combined CloudSat and CALIPSO observations. *Earth System Science Data*, 16(3), 1301–1316. https://doi.org/10.5194/essd-16-1301-2024

Boehm, M. T., & Verlinde, J. (2000). Stratospheric influence on upper tropospheric tropical cirrus. Geophysical Research Letters, 27(19), 3209–3212. https://doi.org/10.1029/2000GL011678

Bourassa, A. E., Degenstein, D. A., & Llewellyn, E. J. (2005). Climatology of the subvisual cirrus clouds as seen by OSIRIS on Odin. Advances in Space Research, 36(5), 807–812. https://doi.org/10.1016/j.asr.2005.05.045

Chen, Q.-X., Huang, C.-L., Dong, S.-K., & Lin, K.-F. (2024). Satellite-based background aerosol optical depth determination via global statistical analysis of multiple lognormal distribution. *Remote Sensing*, 16(7), 1210. https://doi.org/10.3390/rs16071210

Corti, T., Luo, B. P., Fu, Q., Vömel, H., & Peter, T. (2006). The impact of cirrus clouds on tropical troposphere-to-stratosphere transport. Atmospheric Chemistry and Physics, 6(9), 2539–2547. https://doi.org/10.5194/acp-6-2539-2006

MU ET AL. 12 of 14

2576604x, 2025, 6, Downloaded from https

- Deng, M., Mace, G. G., Wang, Z., & Lawson, R. P. (2013). Evaluation of several A-train ice cloud retrieval products with in situ measurements collected during the SPARTICUS campaign. *Journal of Applied Meteorology and Climatology*, 52(4), 1014–1030. https://doi.org/10.1175/JAMC-D-12-054.1
- Deutloff, J., Buehler, S. A., Brath, M., & Naumann, A. K. (2025). Insights on tropical high-cloud radiative effect from a new conceptual model. Journal of Advances in Modeling Earth Systems, 17(2), e2024MS004615. https://doi.org/10.1029/2024MS004615
- Diffenbaugh, N. S., Scherer, M., & Trapp, R. J. (2013). Robust increases in severe thunderstorm environments in response to greenhouse forcing. Proceedings of the National Academy of Sciences, 110(41), 16361–16366. https://doi.org/10.1073/pnas.1307758110
- Dinh, T., & Fueglistaler, S. (2014). Microphysical, radiative, and dynamical impacts of thin cirrus clouds on humidity in the tropical tropopause layer and lower stratosphere. *Geophysical Research Letters*, 41(19), 6949–6955. https://doi.org/10.1002/2014GL061289
- Gasparini, B., Sullivan, S. C., Sokol, A. B., Kärcher, B., Jensen, E., & Hartmann, D. L. (2023). Opinion: Tropical cirrus From micro-scale processes to climate-scale impacts. Atmospheric Chemistry and Physics, 23(24), 15413–15444. https://doi.org/10.5194/acp-23-15413-2023
- Ge, J., Hu, X., Mu, Q., Liu, B., Zhu, Z., Du, J., et al. (2024). Contrasting characteristics of continental and oceanic deep convective systems at different life stages from CloudSat observations. Atmospheric Research, 298, 107157. https://doi.org/10.1016/j.atmosres.2023.107157
- Gelaro, R., McCarty, W., Suárez, M. J., Todling, R., Molod, A., Takacs, L., et al. (2017). The modern-era retrospective analysis for research and applications, version 2 (MERRA-2). *Journal of Climate*, 30(14), 5419–5454. https://doi.org/10.1175/JCLI-D-16-0758.1
- Gill, A. E. (1980). Some simple solutions for heat-induced tropical circulation. *Quarterly Journal of the Royal Meteorological Society*, 106(449), 447–462. https://doi.org/10.1002/qj.49710644905
- Global Modeling And Assimilation Office, & Pawson, S. (2015). MERRA-2 tavg1_2d_lnd_Nx: 2d,1-Hourly,Time-Averaged,Single-Level, Assimilation,Land surface diagnostics V5.12.4 [Dataset]. NASA Goddard Earth Sciences Data and Information Services Center. https://doi.org/10.5067/RKPHT8KC1Y1T
- Gryspeerdt, E., Stettler, M. E. J., Teoh, R., Burkhardt, U., Delovski, T., Driver, O. G. A., & Painemal, D. (2024). Operational differences lead to longer lifetimes of satellite detectable contrails from more fuel efficient aircraft. *Environmental Research Letters*, 19(8), 084059. https://doi.org/10.1088/1748-9326/ad5b78
- Hartmann, D. L., & Berry, S. E. (2017). The balanced radiative effect of tropical anvil clouds. *Journal of Geophysical Research: Atmospheres*, 122(9), 5003–5020. https://doi.org/10.1002/2017JD026460
- Hartmann, D. L., & Larson, K. (2002). An important constraint on tropical cloud climate feedback. *Geophysical Research Letters*, 29(20), 12-1-12-4. https://doi.org/10.1029/2002GL015835
- Heymsfield, A. J., Bansemer, A., Matrosov, S., & Tian, L. (2008). The 94-GHz radar dim band: Relevance to ice cloud properties and CloudSat. Geophysical Research Letters, 35(3), 2007GL031361. https://doi.org/10.1029/2007GL031361
- Hong, Y., Liu, G., & Li, J.-L. F. (2016). Assessing the radiative effects of global ice clouds based on CloudSat and CALIPSO measurements.
- Journal of Climate, 29(21), 7651–7674. https://doi.org/10.1175/JCLI-D-15-0799.1

 Horner, G., & Gryspeerdt, E. (2023). The evolution of deep convective systems and their associated cirrus outflows. Atmospheric Chemistry and
- Physics, 23(22), 14239–14253. https://doi.org/10.5194/acp-23-14239-2023

 Hu, X., Ge, J., Li, W., Du, J., Li, Q., & Mu, Q. (2021). Vertical structure of tropical deep convective systems at different life stages from CloudSat
- observations. Journal of Geophysical Research: Atmospheres, 126(21), e2021JD035115. https://doi.org/10.1029/2021JD035115

 Jensen, E. J., Pfister, L., & Toon, O. B. (2011). Impact of radiative heating, wind shear, temperature variability, and microphysical processes on the structure and evolution of thin cirrus in the tropical tropopause layer. Journal of Geophysical Research, 116(D12), D12209. https://doi.org/10.1029/2010JD015417
- Joos, H., Spichtinger, P., Lohmann, U., Gayet, J.-F., & Minikin, A. (2008). Orographic cirrus in the global climate model ECHAM5. *Journal of Geophysical Research*, 113(D18). https://doi.org/10.1029/2007JD009605
- Krämer, M., Rolf, C., Luebke, A., Afchine, A., Spelten, N., Costa, A., et al. (2016). A microphysics guide to cirrus clouds Part 1: Cirrus types. Atmospheric Chemistry and Physics, 16(5), 3463–3483. https://doi.org/10.5194/acp-16-3463-2016
- Lamraoui, F., Krämer, M., Afchine, A., Sokol, A. B., Khaykin, S., Pandey, A., & Kuang, Z. (2023). Sensitivity of convectively driven tropical tropopause cirrus properties to ice habits in high-resolution simulations. *Atmospheric Chemistry and Physics*, 23(4), 2393–2419. https://doi.org/10.5194/acp-23-2393-2023
- Lesigne, T., Ravetta, F., Podglajen, A., Mariage, V., & Pelon, J. (2024). Extensive coverage of ultrathin tropical tropopause layer cirrus clouds revealed by balloon-borne lidar observations. *Atmospheric Chemistry and Physics*, 24(10), 5935–5952. https://doi.org/10.5194/acp-24-5935-
- Li, J., Lv, Q., Jian, B., Zhang, M., Zhao, C., Fu, Q., et al. (2018). The impact of atmospheric stability and wind shear on vertical cloud overlap over the Tibetan Plateau. Atmospheric Chemistry and Physics, 18(10), 7329–7343. https://doi.org/10.5194/acp-18-7329-2018
- Li, Y., Thompson, D. W. J., Stephens, G. L., & Bony, S. (2014). A global survey of the instantaneous linkages between cloud vertical structure and large-scale climate. *Journal of Geophysical Research: Atmospheres*, 119(7), 3770–3792. https://doi.org/10.1002/2013JD020669
- Luebke, A. E., Afchine, A., Costa, A., Grooß, J.-U., Meyer, J., Rolf, C., et al. (2016). The origin of midlatitude ice clouds and the resulting influence on their microphysical properties. *Atmospheric Chemistry and Physics*, 16(9), 5793–5809. https://doi.org/10.5194/acp-16-5793-2016
- Mace, G. G., Benson, S., & Vernon, E. (2006). Cirrus clouds and the large-scale atmospheric state: Relationships revealed by six years of ground-based data. *Journal of Climate*, 19(13), 3257–3278. https://doi.org/10.1175/JCLI3786.1
- Matsuno, T. (1966). Quasi-geostrophic motions in the equatorial area. *Journal of the Meteorological Society of Japan. Ser. II*, 44(1), 25–43. https://doi.org/10.2151/jmsj1965.44.1 25
- Matus, A. V., & L'Ecuyer, T. S. (2017). The role of cloud phase in earth's radiation budget. *Journal of Geophysical Research: Atmospheres*, 122(5), 2559–2578. https://doi.org/10.1002/2016JD025951
- McKim, B., Bony, S., & Dufresne, J.-L. (2024). Weak anvil cloud area feedback suggested by physical and observational constraints. *Nature Geoscience*, 17(5), 392–397. https://doi.org/10.1038/s41561-024-01414-4
- Mu, Q. (2025). muqingyu666/CirrusClassify-MeteAnalysis: Code data for manuscript requirements, etc. (official) [Collection]. Zenodo. https://doi.org/10.5281/zenodo.17268605
- Riihimaki, L. D., & McFarlane, S. A. (2010). Frequency and morphology of tropical tropopause layer cirrus from CALIPSO observations: Are isolated cirrus different from those connected to deep convection? *Journal of Geophysical Research*, 115(D18), 2009JD013133. https://doi.org/10.1029/2009JD013133
- Sassen, K., Wang, Z., & Liu, D. (2008). Global distribution of cirrus clouds from CloudSat/Cloud-Aerosol Lidar and Infrared Pathfinder Satellite Observations (CALIPSO) measurements. *Journal of Geophysical Research*, 113(D8), 2008JD009972. https://doi.org/10.1029/2008JD009972
- Singh, D. K., Sanyal, S., & Wuebbles, D. J. (2024). Understanding the role of contrails and contrail cirrus in climate change: A global perspective. Atmospheric Chemistry and Physics, 24(16), 9219–9262. https://doi.org/10.5194/acp-24-9219-2024

MU ET AL. 13 of 14

- 2576604x, 2025, 6, Downloaded from https com/doi/10.1029/2025AV001919 by Lanzhou University, Wiley Online Library on [05/11/2025]. See the Terms -conditions) on Wiley Online Library for rules of use; OA articles are governed by the applicable Creative Co
- Sokol, A. B., & Hartmann, D. L. (2020). Tropical anvil clouds: Radiative driving toward a preferred state. *Journal of Geophysical Research:* Atmospheres, 125(21), e2020JD033107. https://doi.org/10.1029/2020JD033107
- Sokol, A. B., Wall, C. J., & Hartmann, D. L. (2024). Greater climate sensitivity implied by anvil cloud thinning. *Nature Geoscience*, 17(5), 398–403. https://doi.org/10.1038/s41561-024-01420-6
- Teoh, R., Engberg, Z., Schumann, U., Voigt, C., Shapiro, M., Rohs, S., & Stettler, M. E. J. (2024). Global aviation contrail climate effects from 2019 to 2021. Atmospheric Chemistry and Physics, 24(10), 6071–6093. https://doi.org/10.5194/acp-24-6071-2024
- Virts, K. S., & Wallace, J. M. (2014). Observations of temperature, wind, cirrus, and trace gases in the tropical tropopause transition layer during the MJO. *Journal of the Atmospheric Sciences*, 71(3), 1143–1157. https://doi.org/10.1175/JAS-D-13-0178.1
- Wheeler, M., & Kiladis, G. N. (1999). Convectively coupled equatorial waves: Analysis of clouds and temperature in the wavenumber–frequency domain. Retrieved from https://journals.ametsoc.org/view/journals/atsc/56/3/1520-0469_1999_056_0374_ccewao_2.0.co_2.xml
- Zhang, G. (2023). Warming-induced contraction of tropical convection delays and reduces tropical cyclone formation. *Nature Communications*, 14(1), 6274. https://doi.org/10.1038/s41467-023-41911-5
- Zhao, B., Wang, Y., Gu, Y., Liou, K.-N., Jiang, J. H., Fan, J., et al. (2019). Ice nucleation by aerosols from anthropogenic pollution. *Nature Geoscience*, 12(8), 602–607. https://doi.org/10.1038/s41561-019-0389-4

MU ET AL. 14 of 14